Optical conductivity of the Hubbard chain away from half filling

Alexander C. Tiegel,[1] Thomas Veness,[2] Piet E. Dargel,[1] Andreas Honecker,[3]
Thomas Pruschke,[1] Ian P. McCulloch,[4] and Fabian H. L. Essler[2]

[1] *Institut für Theoretische Physik, Georg-August-Universität Göttingen, 37077 Göttingen, Germany*
[2] *The Rudolf Peierls Centre for Theoretical Physics, University of Oxford, Oxford, OX1 3NP, United Kingdom*
[3] *Laboratoire de Physique Théorique et Modélisation, CNRS UMR 8089, Université de Cergy-Pontoise, 95302 Cergy-Pontoise Cedex, France*
[4] *Centre for Engineered Quantum Systems, School of Physical Sciences, The University of Queensland, Brisbane, Queensland 4072, Australia*

(Dated: January 6, 2016)

We consider the optical conductivity $\sigma_1(\omega)$ in the metallic phase of the one-dimensional Hubbard model. Our results focus on the vicinity of half filling and the frequency regime around the optical gap in the Mott insulating phase. By means of a density-matrix renormalization group implementation of the correction-vector approach, $\sigma_1(\omega)$ is computed for a range of interaction strengths and dopings. We identify an energy scale $E_{\rm opt}$ above which the optical conductivity shows a rapid increase. We then use a mobile impurity model in combination with exact results to determine the behavior of $\sigma_1(\omega)$ for frequencies just above $E_{\rm opt}$ which is in agreement with our numerical data. As a main result, we find that this onset behavior is not described by a power law.

I. INTRODUCTION

The Mott metal-insulator transition is a paradigm for the importance of electron-electron interactions in correlated many-particle systems. It occurs in a range of materials and has attracted much attention over the last fifty years.[1,2] While the mechanism that drives the transition is well understood, some of the dynamical properties relating to Mott physics remain to be fully explored. A characteristic feature of the Mott phase is the interaction-induced formation of an excitation gap.[2] This gap is visible in various dynamical correlation functions such as the real part $\sigma_1(\omega)$ of the optical conductivity

$$\sigma_1(\omega) = -\frac{\mathrm{Im}\,\chi^J(\omega)}{\omega}, \tag{1}$$

$$\chi^J(\omega) = -\frac{ie^2}{L}\int_0^\infty \mathrm{d}t\; e^{i\omega t}\langle GS|[J(t),J(0)]|GS\rangle. \tag{2}$$

Here $J=\sum_j J_j$ is the current operator

$$J_j = -it\sum_\sigma \left[c^\dagger_{j,\sigma}c_{j+1,\sigma} - c^\dagger_{j+1,\sigma}c_{j,\sigma}\right]. \tag{3}$$

The Mott gap disappears upon doping, and an interesting question is what $\sigma_1(\omega)$ looks like in the metallic phase close to the Mott transition. Here we investigate this issue in one spatial dimension for the archetypal example of the Mott transition, the Hubbard model[3]

$$H = -t\sum_{j,\sigma}\left[c^\dagger_{j+1,\sigma}c_{j,\sigma} + c^\dagger_{j,\sigma}c_{j+1,\sigma}\right] + U\sum_j n_{j,\uparrow}n_{j,\downarrow} - \mu\sum_j\left[n_{j,\uparrow}+n_{j,\downarrow}\right]. \tag{4}$$

Here, $c_{j,\sigma}$ annihilates a fermion with spin $\sigma=\uparrow,\downarrow$ at site j, $n_{j,\sigma}=c^\dagger_{j,\sigma}c_{j,\sigma}$ is the number operator, t is the hopping parameter which is set to $t=1$ in our calculations, μ is the chemical potential, and $U\geq 0$ is the strength of the on-site repulsion.

At zero temperature and half filling the optical conductivity has been comprehensively analyzed by both analytic and numerical methods:[4–7] the system is insulating and there is an optical gap[8] at $\omega=2\Delta$, i.e., twice the Mott-Hubbard gap, below which the optical conductivity vanishes. Immediately above this gap, $\sigma_1(\omega)$ exhibits a square-root increase. In contrast, much less is known regarding the optical conductivity away from half filling. In the thermodynamic limit, the optical conductivity consists of a delta peak at zero frequency, the Drude peak, and a so-called regular or incoherent part

$$\sigma_1(\omega\geq 0) = D\,\delta(\omega) + \sigma^{\rm reg}(\omega). \tag{5}$$

The low-frequency behavior has been studied using methods based on Luttinger liquid theory,[9–11] which predict a universal ω^3 behavior of $\sigma^{\rm reg}(\omega)$ at $0<\omega\ll t$. Moreover, in the case of one doped hole at strong coupling ($U\gg 1$), an $\omega^{3/2}$ dependence at small frequency and spectral weight in the region $0<\omega<4t$ have been reported.[12]. However, it is clear on general grounds that at low dopings, i.e. $1-n\ll 1$, only a minute fraction of the total spectral weight in $\sigma_1(\omega)$ will be associated with features at frequencies below the optical gap 2Δ at half filling. One expects there to be a characteristic "pseudogap" energy scale $E_{\rm opt}$ above which $\sigma_1(\omega)$ will increase and exhibit a similar behavior to the one seen at half filling. The low-intensity features below $E_{\rm opt}$ involve only excitations comprising of holon-antiholon pairs. The scale $E_{\rm opt}$ has been identified in a work by Carmelo *et al.*[13] and is obtained from the Bethe ansatz solution of the one-dimensional Hubbard model.[3] In Fig. 1 we present results for $E_{\rm opt}$ as a function of the band filling for several values of U.

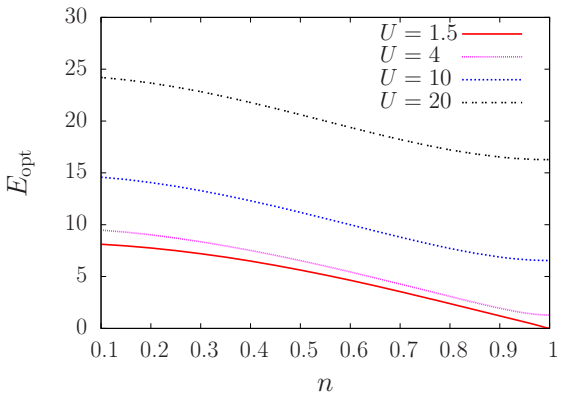

FIG. 1. (Color online) Bethe ansatz results for theoretical "pseudogap" onset value[13,14] $E_{\rm opt}$ as a function of U and n.

In Ref. 13 it was conjectured that the optical conductivity increases in a power-law fashion above $E_{\rm opt}$

$$\sigma_1(\omega) \sim (\omega - E_{\rm opt})^{\zeta}\ \Theta(\omega - E_{\rm opt})\ . \qquad (6)$$

In the following we investigate the behavior of the optical conductivity for small dopings, paying particular attention to its behavior above the pseudogap. Our analysis is based on a combination of density-matrix renormalization group (DMRG) computations[15] and results obtained by employing a mobile impurity model description[14,16–21] augmented by exact Bethe Ansatz calculations.

The paper is organized as follows. We briefly review the DMRG-based correction-vector approach in Sec. II and present our numerical results in Sec. III. The frequency dependence of $\sigma_1(\omega)$ above $E_{\rm opt}$ is also determined by means of a mobile impurity model (MIM) in combination with exact results in Sec. IV. Section V provides a comparison of our DMRG and MIM calculations, which shows that the onset behavior directly above $E_{\rm opt}$ is not described by a power law. Finally, our conclusions are summarized in Sec. VI.

II. NUMERICAL METHOD.

We use a matrix product state (MPS)[22,23] implementation of the correction-vector approach,[24] which is an extension of the DMRG to compute spectral functions. There exist several variants of this correction-vector approach[25–27] such as DDMRG.[5] We can recast Eq. (1) as

$$\sigma_1(\omega > 0) = -\lim_{\eta\to 0^+} \frac{e^2}{\omega L}\ {\rm Im}\ G_J(\omega > 0, \eta), \qquad (7)$$

where

$$G_J(\omega,\eta) = \langle GS|J^\dagger\ \frac{1}{\omega + i\eta - (H - E_{GS})}\ J|GS\rangle. \qquad (8)$$

Here E_{GS} is the ground-state energy. The correction vector is defined by

$$|\psi_J(\omega,\eta)\rangle = \frac{1}{E_{GS} + \omega + i\eta - H} J|GS\rangle, \qquad (9)$$

and can be obtained as the solution $|\psi\rangle$ of the linear system

$$(E_{GS} + \omega + i\eta - H)|\psi\rangle = J|GS\rangle. \qquad (10)$$

Here the basic idea is to variationally determine the correction vector associated with $G_J(\omega,\eta)$ at the frequency of interest within the ansatz class of MPS. We solve this set of equations directly by local updates of the MPS $|\psi\rangle$ (see Ref. 28 for details). Sweeping through the chain in a DMRG-like fashion until convergence is reached, a local non-Hermitian system of equations is solved at each site by the generalized minimal residual (GMRES) method.[29] The dynamical correlation function can be evaluated as the overlap $G_J(\omega,\eta) = \langle GS|J^\dagger|\psi_J(\omega,\eta)\rangle$. Note that the correction vector needs to be computed separately for each frequency ω. Importantly, the method gives intrinsically broadened results with a Lorentzian line shape of width $\eta > 0$, which is crucial for Eq. (10) to be well-conditioned. The correction-vector calculations are performed for chains of up to $L = 84$ sites and open boundary conditions (OBCs). Finite-size effects cause the spectral weight of the Drude peak to be redistributed to finite frequencies above the lowest energy scale $\sim 1/L$.[30] By considering sufficiently large U, these effects are well-separated from the onset at the edge of the "pseudogap". To obtain accurate results, we exploit the $SU(2)$ symmetry[23] of the Hamiltonian (4) and keep $m = 1300$ DMRG states for ground-state calculations. For the dynamics, $m = 500$ states were retained for the correction-vector approach at a filling of $n = 1$ and at $n < 1$, $m = 600$.

III. RESULTS FOR THE ABSORPTION BAND.

A well-defined absorption band above $E_{\rm opt}$ is only observed for sufficiently large values of the repulsion U. Moreover, far from half filling, e.g. at quarter-filling ($n = 1/2$), almost all of the intensity is contained in the Drude peak.[31] Therefore, the DMRG results for $\sigma_1(\omega)$ in Fig. 2 are obtained for $U = 6$ and 16 and a filling factor not smaller than $n = 2/3$. Finite-size and boundary condition effects are dominated by the intrinsic broadening introduced due to $\eta = 0.2$. Only the $n = 2/3$ curve in the upper panel of Fig. 2 displays a slight increase towards small frequencies. This increase is mainly a consequence of the Drude peak appearing at finite frequencies for OBCs[30] and the growing Drude weight for a fixed value of U with increasing doping. Moreover, it is observed that for a given U the integrated spectral weight below the regular part decreases with increasing doping. This is in qualitative agreement with exact results for the

relative weight of Drude peak with respect to the total intensity for an infinite system.[31] In the thermodynamic limit, the Drude peak vanishes at half filling; this transfer of spectral weight to finite frequencies as a function of n is very sharp for small and extremely large U and can be understood in terms of umklapp processes.[31] The two spectra at half filling ($n = 1$) shown in Fig. 2 are in agreement with the U dependence of the Mott-Hubbard gap Δ.[3] With decreasing filling n, the frequency at which $\sigma_1(\omega)$ becomes sizable for a given U increases compared to 2Δ. The rapid increase of the DMRG results above this frequency agrees well with existing results for $E_{\rm opt}$,[13] which are marked by arrows in Fig. 2. The broadened spectra also suggest that the onset at the lower threshold becomes softer for decreasing filling and the upper band edge does not vary significantly for different fillings. This softening can be understood in terms of the mobile impurity approach discussed below. The results in Fig. 2 confirm the expectation that the optical spectra become more symmetric for higher values of U.[4,13] The

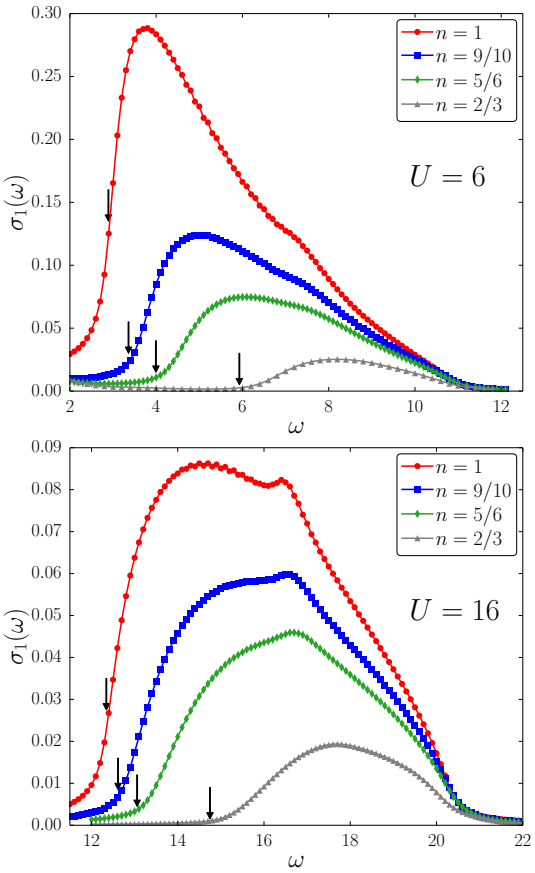

FIG. 2. (Color online) DMRG results for the regular part of the optical conductivity show a well-defined absorption band for various fillings n and a Lorentzian broadening of $\eta = 0.2$. The data are obtained for a chain of $L = 60$ and OBCs. (Upper panel) $U = 6$. (Lower panel) $U = 16$. The arrows mark the results for $E_{\rm opt}$ determined by Bethe ansatz. Note that the ω-axis starts at different frequencies in both panels.

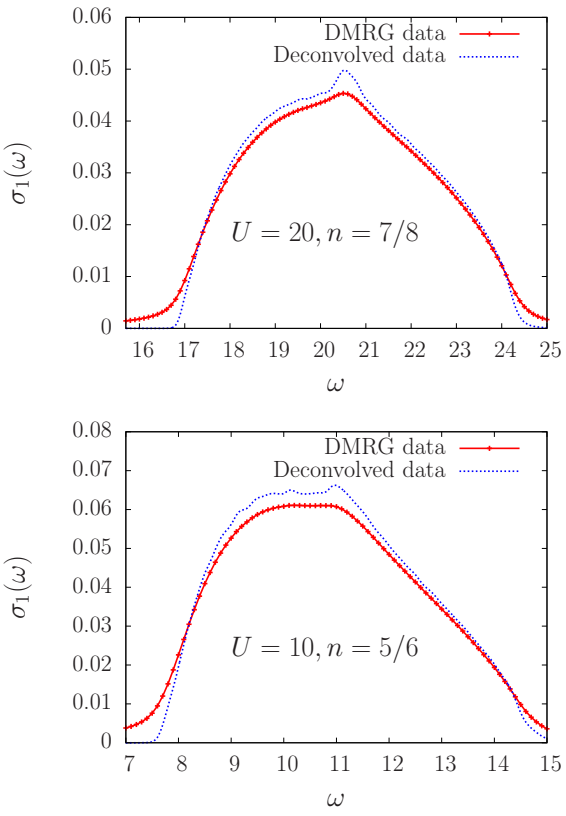

FIG. 3. (Color online) DMRG results with an intrinsic Lorentzian broadening of $\eta = 0.2$ are compared to the corresponding deconvolved data. (Upper panel) $U = 20$, $n = 7/8$, and $L = 80$. (Lower panel) $U = 10$, $n = 5/6$, and $L = 84$.

small peak in the middle of the absorption band is very similar to the one previously observed at half filling,[4] and has its origin in the large density of states for excitations between parallel bands. Its existence is evident for $U = 16$ and it can still be observed as a weak feature for $U = 6$. For $U = 16$ the small peak is found to persist at least down to $n = 5/6$.

In order to compare our DMRG results to the prediction of the mobile impurity model (MIM) presented in the next section, it is necessary to remove the intrinsic Lorentzian broadening of the DMRG data. This a numerically ill-conditioned problem, but in practice the following procedure was found to work reliably. The initial correction-vector results are obtained on a grid of frequencies separated by $\Delta\omega = 0.1$. We use rational functions to both interpolate and extrapolate this data.[32] The resulting continuous function is then deconvolved using the Richardson-Lucy algorithm.[33,34] Comparisons of the inherently broadened DMRG results and the deconvolved data are presented in Fig. 3, where the onset behavior is smooth, but small artefacts can be seen at higher frequencies.

IV. MOBILE IMPURITY MODEL (MIM).

While the low-energy sector of the Hubbard model is described by a spin-charge separated Luttinger liquid (LL), the calculation of finite-frequency properties requires a careful treatment of perturbations. Perturbation theory in some of these irrelevant operators exhibits infrared singularities, which lead to strong deviations from LL behavior. Crucially, in the vicinity of thresholds for simple excitations the problem can be mapped to that of a high-energy mobile impurity coupled to a LL.[16,17] The parameters of this MIM can be completely determined by using exact results obtained in the framework of the Bethe ansatz solution.[18] The appropriate model for the optical conductivity at frequencies just above $E_{\rm opt}$ can be cast in the form $H=\int dx[\mathcal{H}_{\rm LL}+\mathcal{H}_{\rm imp}+\mathcal{H}_{\rm int}]$, where[14,20]

$$\begin{aligned}\mathcal{H}_{\rm LL}&=\sum_{\alpha=c,s}\frac{v_\alpha}{16\pi}\left[\frac{1}{2K_\alpha}\left(\partial_x\Phi^*_\alpha\right)^2+2K_\alpha\left(\partial_x\Theta^*_\alpha\right)^2\right],\\ \mathcal{H}_{\rm imp}&=B^\dagger(x)\left[\varepsilon(0)-\frac{1}{2}\varepsilon''(0)\partial_x^2\right]B(x)\ ,\\ \mathcal{H}_{\rm int}&=B^\dagger(x)B(x)\left[f_\alpha\partial_x\varphi^*_\alpha(x)+\bar f_\alpha\partial_x\bar\varphi^*_\alpha(x)\right].\end{aligned}\tag{11}$$

Here the Luttinger liquid part $\mathcal{H}_{\rm LL}$ describes the low-energy spin and charge collective modes, whereas $\mathcal{H}_{\rm imp}$ is the Hamiltonian of a high-energy "impurity" with quadratically decreasing dispersion $\varepsilon(p)$ around zero momentum. Finally $\mathcal{H}_{\rm int}$ describes the interaction of the impurity with the low-energy degrees of freedom. The parameters $v_{c,s}$, $K_{c,s}$, $f_{c,s}$, $\bar f_{c,s}$ and $\varepsilon(q)$ in (11) can be determined from the Bethe ansatz solution.[14] The physical content of the model (11) is as follows. Excitations at frequencies just above $E_{\rm opt}$ consist of a single high-energy bound state (k-Λ string[3]) and a number of low-energy excitations.[13] Assuming the bound state to be a point-like object and retaining only the most relevant interactions in $\mathcal{H}_{\rm int}$ then leads to the model (11). The current operator (3) can be projected on the MIM degrees of freedom[14]

$$J_j\to\left(\partial_xB^\dagger(x)\right)e^{-i\Theta^*_c(x)/\sqrt{2}}\sin\left(\frac{\Phi^*_s}{2\sqrt{2}}\right)+\dots\tag{12}$$

The calculation of the current-current correlation function, and thus the optical conductivity in the framework of the MIM (11), then proceeds along standard lines[16] and results in an expression of the form

$$\begin{aligned}\sigma_1(\omega\approx E_{\rm opt})\sim\frac{C}{\omega}\int_{-\Lambda}^{\Lambda}{\rm d}p\Big\{&\frac{\gamma_c^2}{K_c}\left((1+\gamma)\left[\widetilde G^c_{\gamma+2,\gamma}(\omega,p)+\widetilde G^c_{\gamma,\gamma+2}(\omega,p)\right]-2\gamma\widetilde G^c_{\gamma+1,\gamma+1}(\omega,p)\right)\\&+\sqrt{\frac{4\gamma}{K_c}}\gamma_cp\left[\widetilde G^c_{\gamma+1,\gamma}(\omega,p)-\widetilde G^c_{\gamma,\gamma+1}(\omega,p)\right]+p^2\widetilde G^c_{\gamma,\gamma}(\omega,p)+\gamma_s^2\widetilde G^s_{\gamma}(\omega,p)\Big\},\end{aligned}\tag{13}$$

where

$$\widetilde G^c_{\gamma,\delta}(\omega,p)=\frac{(2\pi)^2\Theta(\omega_c(|p|))(\omega_c(-p))^{\gamma-1}(\omega_c(p))^{\delta-1}}{\Gamma(\gamma)\Gamma(\delta)(2v_c)^{\gamma+\delta-1}},\tag{14}$$

$$\begin{aligned}\widetilde G^s_{\gamma}(\omega,p)=&\frac{(2\pi)^2(\omega_s(p))^{2\gamma-1}}{\Gamma^2(\gamma)(v_c^2-v_s^2)^\gamma}\Theta(\omega_s(p))\int_0^1{\rm d}s\,s^{\gamma-1}\\&\times(1-s)^{\gamma-1}\left[\frac{2v_c(\omega-v_sp)}{v_c^2-v_s^2}s-\frac{\omega_c(p)}{v_c-v_s}\right]\\&\times\Theta\Big(\frac{2v_c\omega_s(p)}{v_c^2-v_s^2}s-\frac{\omega_c(p)}{v_c-v_s}\Big)+p\to-p.\end{aligned}\tag{15}$$

Here we have defined $\omega_\alpha(p)=\omega-\varepsilon(p)-v_\alpha p$ and Λ is a cutoff. The parameter γ is shown in Fig. 4 as a function of band filling for several values of U. The result (13) applies in an a priori unknown frequency window above $E_{\rm opt}$. This energy window shrinks to zero as we approach half filling $n\to1$, and the behavior of (13) is in fact very different from the square-root increase seen at half filling.

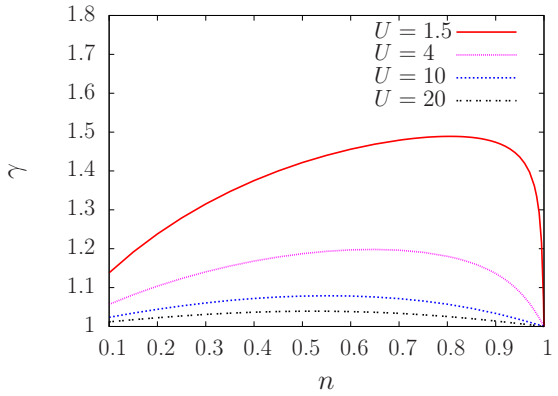

FIG. 4. (Color online) Parameter γ as a function of U and n.

V. BEHAVIOR OF $\sigma_1(\omega)$ ABOVE THE CROSS-OVER SCALE $E_{\rm opt}$

Focusing on frequencies in the vicinity of $E_{\rm opt}$ in Fig. 3, we observe that the deconvolved DMRG data exhibits a smooth and slow increase. This behavior can be directly compared to the results obtained from the MIM. In the

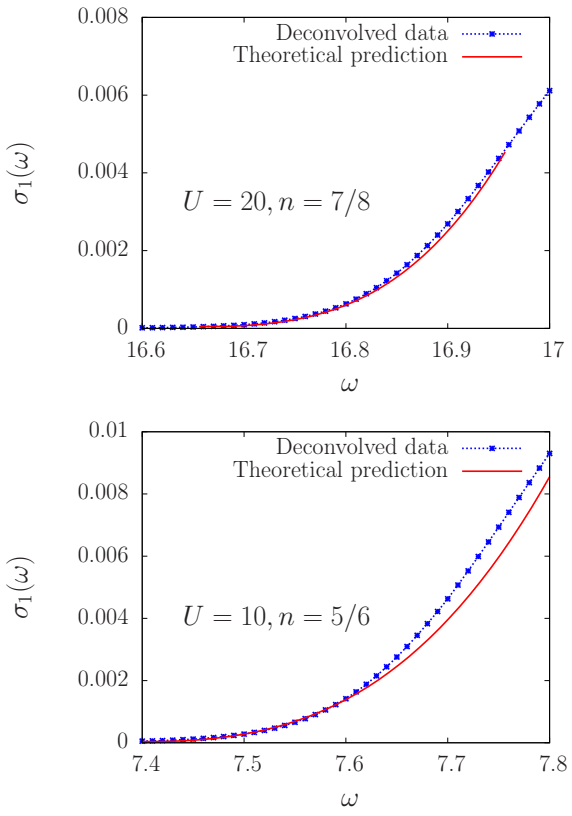

FIG. 5. (Color online) Comparison of theoretical predictions from a mobile impurity model with numerical results from DMRG.

latter we adjust the overall amplitude C allowing for a small, constant contribution attributed to excitations involving only holons and antiholons which give rise to the Drude peak at zero frequency, but are expected to make up only a small fraction of the spectral weight at $\omega \approx E_{\rm opt}$. We furthermore adapt the cut-off Λ, although the results depend only weakly on it. The comparison in Fig. 5 shows that the MIM results are consistent with the deconvolved DMRG data. Moreover, the increase in $\sigma_1(\omega)$ above $E_{\rm opt}$ is not described by a power law. On a technical level this can be traced back to the fact that the mobile impurity sits at a maximum of its dispersion relation. The results obtained by means of the MIM are very different from the power-law increase (6) predicted in Ref. 13. In particular the exponent ζ predicted in this previous work becomes less than one for $U > 4$, which is not consistent with our deconvolved DMRG data.

VI. CONCLUSIONS.

We have studied the real part $\sigma_1(\omega)$ of the zero temperature optical conductivity in the one-dimensional Hubbard model in the metallic phase close to half filling. At half filling $n = 1$, it is known that $\sigma_1(\omega)$ vanishes below twice the Mott gap, and then increases in a characteristic square-root fashion.[4] Doping away from half filling induces a Drude peak at zero frequency, the weight of which scales with $1 - n$. Here we have focused on frequency scales close to the optical gap at half filling, and investigated how $\sigma_1(\omega)$ gets modified upon doping holes into the system. In our DMRG calculations, we have observed a rapid increase above a cross-over scale $E_{\rm opt}$, and analyzed this behavior in the framework of a mobile impurity model. The results obtained by this method were found to be in agreement with our DMRG data. Therefore, the increase of $\sigma_1(\omega)$ for frequencies above the pseudogap $E_{\rm opt}$, in which only small-amplitude excitations comprising of holon-antiholon pairs are present, is not described by a power law.

ACKNOWLEDGMENTS

We thank Imke Schneider for helpful discussions and collaboration in the early stages of this work. We acknowledge the support by the Helmholtz Gemeinschaft via the Virtual Institute "New states of matter and their excitations" (Project No. VH-VI-521). This work was supported by the EPSRC under grants EP/I032487/1 and EP/J014885/1 (FHLE and TV). IPM acknowledges the support from the Australian Research Council Centre of Excellence for Engineered Quantum Systems, CE110001013, and the srtFuture Fellowships scheme, FT100100515.

[1] N. F. Mott, *Metal-Insulator Transitions*, 2nd ed. (Taylor and Francis, London, 1990).
[2] F. Gebhard, *The Mott Metal-Insulator Transition* (Springer, Berlin, 1997).
[3] F. H. L. Essler, H. Frahm, F. Göhmann, A. Klümper, and V. E. Korepin, *The One-Dimensional Hubbard Model* (Cambridge University Press, Cambridge, 2005).
[4] E. Jeckelmann, F. Gebhard, and F. H. L. Essler, Phys. Rev. Lett. **85**, 3910 (2000).
[5] E. Jeckelmann, Phys. Rev. B **66**, 045114 (2002).
[6] D. Controzzi, F. H. L. Essler, and A. M. Tsvelik, Phys. Rev. Lett. **86**, 680 (2001).
[7] F. H. L. Essler, F. Gebhard, and E. Jeckelmann, Phys. Rev. B **64**, 125119 (2001).
[8] A. A. Ovchinnikov, Sov. Phys. JETP **30**, 1160 (1970).
[9] T. Giamarchi, Phys. Rev. B **44**, 2905 (1991).
[10] T. Giamarchi and A. J. Millis, Phys. Rev. B **46**, 9325 (1992).
[11] T. Giamarchi, Physica B: Cond. Matt. **230**, 975 (1997).
[12] P. Horsch and W. Stephan, Phys. Rev. B **48**, 10595 (1993).

[13] J. M. P. Carmelo, N. M. R. Peres, and P. D. Sacramento, Phys. Rev. Lett. **84**, 4673 (2000).
[14] T. Veness and F. H. L. Essler, in preparation.
[15] S. R. White, Phys. Rev. Lett. **69**, 2863 (1992); S. R. White, Phys. Rev. B **48**, 10345 (1993).
[16] T. L. Schmidt, A. Imambekov, and L. I. Glazman, Phys. Rev. Lett. **104**, 116403 (2010); T. L. Schmidt, A. Imambekov, and L. I. Glazman, Phys. Rev. B **82** 245104 (2010); A. Imambekov, T. L. Schmidt, and L. I. Glazman, Rev. Mod. Phys **84**, 1253 (2012).
[17] R. G. Pereira and E. Sela, Phys. Rev. B **82**, 115324 (2010).
[18] F. H. L. Essler, Phys. Rev. B **81**, 205120 (2010).
[19] R. G. Pereira, K. Penc, S. R. White, P. D. Sacramento, J. M. P. Carmelo, Phys. Rev. B **85**, 165132 (2012).
[20] F. H. L. Essler, R. G. Pereira, and I. Schneider, Phys. Rev. B **91**, 245150 (2015).
[21] L. Seabra, F. H. L. Essler, F. Pollmann, I. Schneider, and T. Veness, Phys. Rev. B **90**, 245127 (2014).
[22] U. Schollwöck, Ann. Phys. **326**, 96 (2011).
[23] I. P. McCulloch, J. Stat. Mech. P10014 (2007).
[24] Z. G. Soos and S. Ramasesha, J. Chem. Phys. **90**, 1067 (1989).
[25] S. Ramasesha, S. K. Pati, H. R. Krishnamurthy, Z. Shuai, and J. L. Brédas, Phys. Rev. B **54**, 7598 (1996).
[26] T. D. Kühner and S. R. White, Phys. Rev. B **60**, 335 (1999).
[27] A. Weichselbaum, F. Verstraete, U. Schollwöck, J. I. Cirac, and J. von Delft, Phys. Rev. B **80**, 165117 (2009).
[28] A. M. Holzner, PhD Thesis, Ludwig-Maximilians-Universität München (2012).
[29] Y. Saad, *Iterative Methods for Sparse Linear Systems*, 2nd ed. (SIAM, Philadelphia, 2003).
[30] R. M. Fye, M. J. Martins, D. J. Scalapino, J. Wagner, W. Hanke, Phys. Rev. B **44**, 6909 (1991).
[31] H. J. Schulz, Phys. Rev. Lett. **64**, 2831 (1990).
[32] W. H. Press, B. P. Flannery, S. A. Teukolsky, and W. T. Vetterling, *Numerical Recipes* (Cambridge University Press, New York, 1986).
[33] W. Richardson, J. Opt. Soc. Am. **62**, 55 (1972).
[34] L. B. Lucy, Astronomical J. **79**, 745 (1974).